

# Structural phase transition of two-dimensional monolayer SnTe from artificial neural network

Jiale Zhang,<sup>1</sup> Danni Wei,<sup>1</sup> Feng Zhang,<sup>1</sup> Xi Chen,<sup>2</sup> and Dawei Wang<sup>1,\*</sup>

<sup>1</sup>*School of Microelectronics & State Key Laboratory for Mechanical Behavior of Materials, Xi'an Jiaotong University, Xi'an 710049, China*

<sup>2</sup>*Department of Applied Physics, Aalto University, Espoo 00076, Finland*

(Dated: November 30, 2021)

As machine learning becomes increasingly important in engineering and science, it is inevitable that machine learning techniques will be applied to the investigation of materials, and in particular the structural phase transitions common in ferroelectric materials. Here, we build and train an artificial neural network to accurately predict the energy change associated with atom displacements and use the trained artificial neural network in Monte-Carlo simulations on ferroelectric materials to investigate their phase transitions. We apply this approach to two-dimensional monolayer SnTe and show that it can indeed be used to simulate the phase transitions and predict the transition temperature. The artificial neural network, when viewed as a universal mathematical structure, can be readily transferred to the investigation of other ferroelectric materials when training data generated with *ab initio* methods are available.

Ferroelectric materials, which have spontaneous polarizations that can be reversed by an external electric field, constitute a group of functional materials that are important for many applications, e.g., ultrafast switches, phased-array radar, and dynamic random access memories<sup>1</sup>. It is reported that SnTe thin films with a thickness of 1-unit cell (UC, with two layers of atoms) can have stable spontaneous polarization up to 270K, and 2-UC to 4-UC SnTe films also have strong ferroelectric properties at room temperature<sup>2</sup>. The ferroelectricity of this two-dimensional (2D) material makes it a good candidate for applications in promising devices such as high-density memory, nano-sensors<sup>3,4</sup>. To fully understand a ferroelectric material such as SnTe, it is necessary to know if it can indeed experience structural phase transition(s), and if so, the phase transition sequence, and temperature is. It is also important to know the relation between the transition temperature  $T_C$  and other factors, such as strain and the number of layers. Since accurately predicting the phase transition temperature requires large systems, it is usually not possible with a pure *ab initio* approach, i.e., the density functional theory (DFT)<sup>5</sup>. To overcome the limitation of DFT's huge computational cost for large systems, one need to propose empirical formulas to fit the inter-atomic potential energy (or forces) to DFT results using small systems, which is then applied to large systems. For more complex systems such as perovskites, the effective Hamiltonian approach has been a popular method to investigate their static and dynamic properties<sup>6-10</sup>. For such first-principles-based methods to work, empirical formulas or proper effective Hamiltonian (along with the specification of the dynamic variables and the coefficients of the effective Hamiltonian) are needed, neither of which is trivial if the aim is to achieve a general and transferable approach for different systems.

Recent advances in machine learning (ML) offers an alternative approach for the construction of the potential-energy surface (PES) by fitting large data sets from electronic structure calculations with DFT<sup>11,12</sup>. The ML potential, when viewed as an universal mathematical structure, has the advantage that it can be used for very different systems with minimal modification. With such an approach, there is no need to reconstruct the formulas for different systems, while the accuracy of the PES remains satisfactory. It is promising that the

use of ML techniques will combine the advantages of both approaches, i.e., the accuracy of DFT and the efficiency of explicit formulas in obtaining the PES<sup>13</sup>. While the ML approach has been applied to many interesting systems<sup>14-16</sup>, the structural phase transitions induced by atom displacements, which is important in ferroelectric materials, have not been dealt with. In this paper, we develop a neural-network-based approach to treat ferroelectric systems, especially their phase transitions. We note that such structural phase changes usually involve atom displacements within unit cells in crystalline phases, unlike the researches focusing on finding novel structures in liquid and amorphous phases<sup>17-20</sup>.

In order to construct this framework and show its efficacy, we use 2D monolayer SnTe as the prototypical material to ground this approach. It is known that SnTe bulk can have a structural phase transition and the SnTe thin films (of 2 or more layers of atoms) can have a rather high transition temperature (270 K)<sup>2</sup>, however, it is unknown if a *monolayer* SnTe can still have a phase transition when all the atoms are confined to 2D. To address this question, we adopt the ML approach, build artificial neural networks (ANN) suitable for the system with two different types of atoms, and take DFT results as training data for the supervised learning of the ANNs. In this way, we have successfully constructed the PES (with respect to the displacement of atoms) and employed it in Monte-Carlo (MC) simulations, which demonstrate a structural phase transition occurring at  $\sim 260$  K. The approach and the programs we have developed are universal enough that they can be used to investigate different crystals and shed light on their structural phase transitions.

The key ingredient in this approach is to build and train an ANN that can efficiently and accurately predict the energy of a given atomic configuration. A monolayer SnTe has the simple structure as shown in Fig. 1(a) where Sn and Te atoms alternate with each other along both the [100] and [010] directions. To fulfill this mission, the whole architecture has the topology shown in Fig. 1 (b), which is similar to those used by Behler and Parrinell<sup>11,21,22</sup>. More specifically, the total energy  $E$  of the system is the sum of atomic contributions  $E_i$ ,

$$E = \sum_i E_i \quad (1)$$

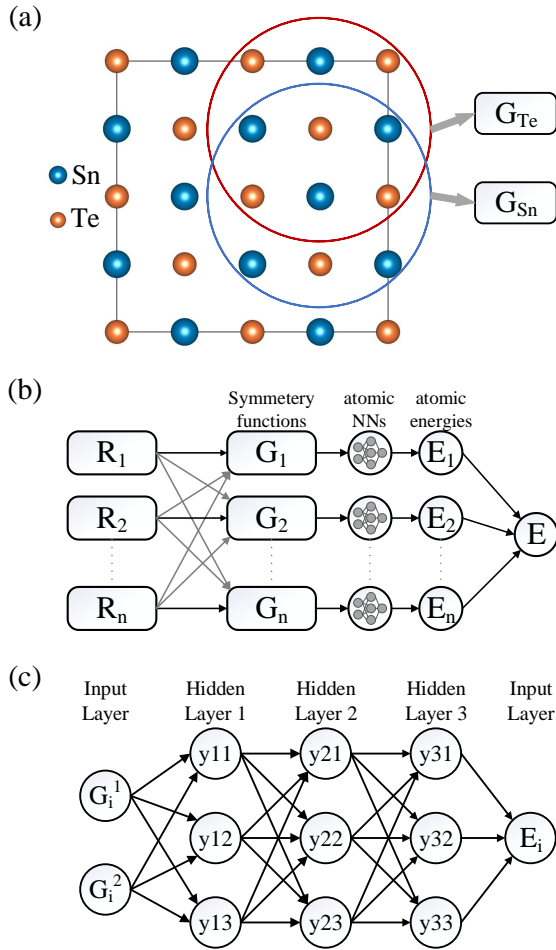


Figure 1. (a) The 2D monolayer SnTe shows alternating Sn and Te atoms along the  $x$  and  $y$  axes. The blue (red) box indicates the chemical environments encircling the Sn (Te) atom at the center; (b) The topology of the whole structure is built to predict the total energy, which contains the ANNs that are schematically shown in (c).

where  $E_i$  is the energy imposed on the  $i$ th atom by its neighboring environment, which will be determined by the ANN we build. It is realized that the inter-atomic potential energy decays rapidly with distance (which is termed the “nearsightedness”<sup>23,24</sup>), therefore a cutoff function is usually used to limit the interaction between atoms to an appropriate range. In this work, we have found that, considering the interaction up to the 5th nearest neighbors [see Fig. 1(a)] will produce satisfactory results. The input to each ANN in Fig. 1(b) is determined by the coordinates of the  $i$ th atom and its eight neighboring atoms, which are encircled in Fig. 1(a) where two situations (Sn in the center and Te in the center) are indicated. For the 2D structure, we only consider atom displacements inside the plane, resulting in an a vector with 18 elements as the input.

To properly and adequately represent the local chemical environment around an atom, we find that it is imperative to use atom-centered symmetry functions  $G$  as descriptors, which

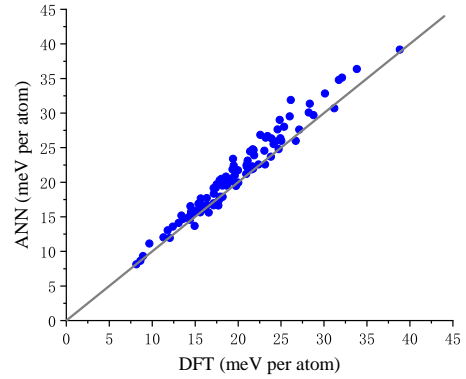


Figure 2. Comparison of the energy predicted by the trained ANN and generated by DFT (using GPAW) where for each data point, its  $x$ -axis value is from GPAW while its  $y$ -axis value is the ANN prediction.

are a series of functions of atom positions<sup>25</sup>. As indicated in Ref. 11, the number of symmetry functions describing a given structure should be greater than the degrees of freedom of the described system so that all information is fully recorded. In Fig. 1(b), the column named “atomic NNs” contains identical ANNs that takes the chemical environment of an atom, which are encoded in  $G$ s as shown by the column named “symmetry functions”, as input and outputs the energy  $E_i$  indicated by the column named “atom energies”. Finally,  $E_i$  is summed to give the total energy  $E$ .

The core components of the whole structure are the ANNs as shown schematically in Fig. 1(c), which can be built with much freedom. For instance, we can use a simple neural network with back-propagation<sup>26</sup> or some deep neural networks<sup>27</sup>. Here, given the relatively simple chemical environments, we constructed an ANN with three hidden layers, each layer containing 40 nodes. In addition, since there are two types of atoms (Sn and Te) in the system, two separate ANNs, which have the same structure but different weights inside its nodes, were established to calculate the two types energies,  $E_{\text{Sn}}$  and  $E_{\text{Te}}$  imposing on Sn and Te atoms, respectively.

We use supervised learning as implemented in PyTorch<sup>28</sup> to train the ANNs, where the DFT calculations are employed to obtain the training data set. Based on the 2D monolayer SnTe, which has the lattice constant  $a_0 = 6.1836 \text{ \AA}$  and a vacuum layer of  $4a_0$  along the  $z$  direction as shown in Fig. 1(a), *ab initio* molecular dynamics simulations with GPAW<sup>29</sup> are performed to simulate a  $2 \times 2$  system (16 atoms) from 500 K to 0 K to generate training samples. Additional configurations with random displacements of atoms are also used to train the model so that it can cope with more complex situations. In these calculations, GPAW uses plane waves with a cutoff energy of 900 eV, a  $2 \times 2 \times 1$  Brillouin-zone sampling grid<sup>30</sup>, and the Perdew-Burke-Ernzerhof (PBE) exchange-correlation functional<sup>31</sup>. A total of about 8000 configurations are calculated, of which 7900 was used to optimize the ANN, and 100 was used as a preliminary test of the predictive ability of the ANNs. For each of the configuration, its energy is calculated

using the energy of the original configuration  $E_O$ , where none of the atoms is displaced, as the energy reference. Figure 2 compares the values predicted by the ANN and calculated by GPAW, which shows a good agreement where the maximum difference is within 6 meV per atom. We note that the energies of the chosen configurations used in Fig. 2 are all higher than  $E_O$ . The prediction by the ANNs for configurations with lower energies agree even better with GPAW as we discuss below (see Fig. 3).

To further verify the accuracy of the ANN, we also generated special configurations where all the Sn atoms are synchronously displaced along a particular direction to a distance  $d$  as shown in Fig. 3(a). We use the trained ANN to predict the energies of these configurations and generate the PES of SnTe as shown in Fig. 3(b). It is interesting to see that the ANN has generated a smooth PES with multiple local energy minimums. To quantitatively check the predictions of the ANN, we have sampled along the  $\langle 110 \rangle$  and the  $\langle 100 \rangle$  directions and compared the energy predicted by the ANN to those calculated with GPAW in Figs. 3(c) and (d). For the region of interest ( $d \leq 0.4 \text{ \AA}$ ), the accuracy provided by the ANN is stunning. It is worth noting that the ANN has successfully reproduced the double-well potential which is a critical indication of possible structural phase transitions<sup>32</sup>. This feat is remarkable when we recall that the ANN has a universal internal structure and is trained with configurations having essentially random atom displacements. While Figs. 3(c) and (d) show that the ANN can fit the PES very well along the  $\langle 100 \rangle$  and the  $\langle 110 \rangle$  directions, one needs to keep in mind that the power of the ANN lies in their ability to predict the energy of *any* configuration, and Figs. 3(b-d) just show some special cases.

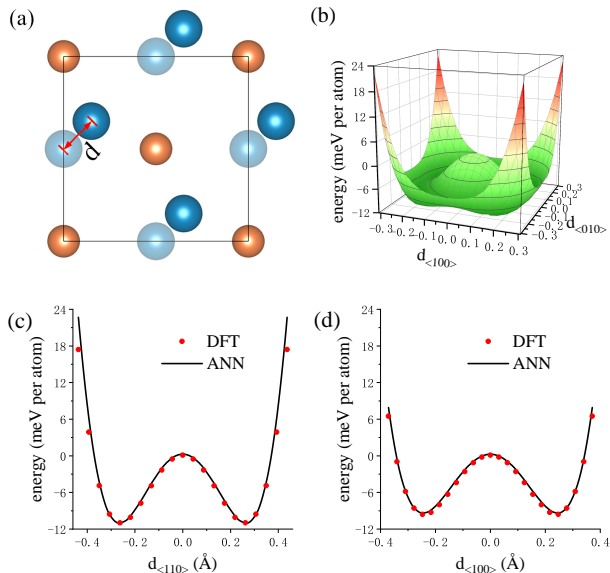


Figure 3. (a) All the Sn atoms in a unit cell move synchronously to a distance  $d$ ; (b) The PES is generated by the ANN, showing multiple energy minimums; (c) and (d) compares the values predicted by the ANN along the  $\langle 110 \rangle$  and the  $\langle 100 \rangle$  directions to the GPAW results.

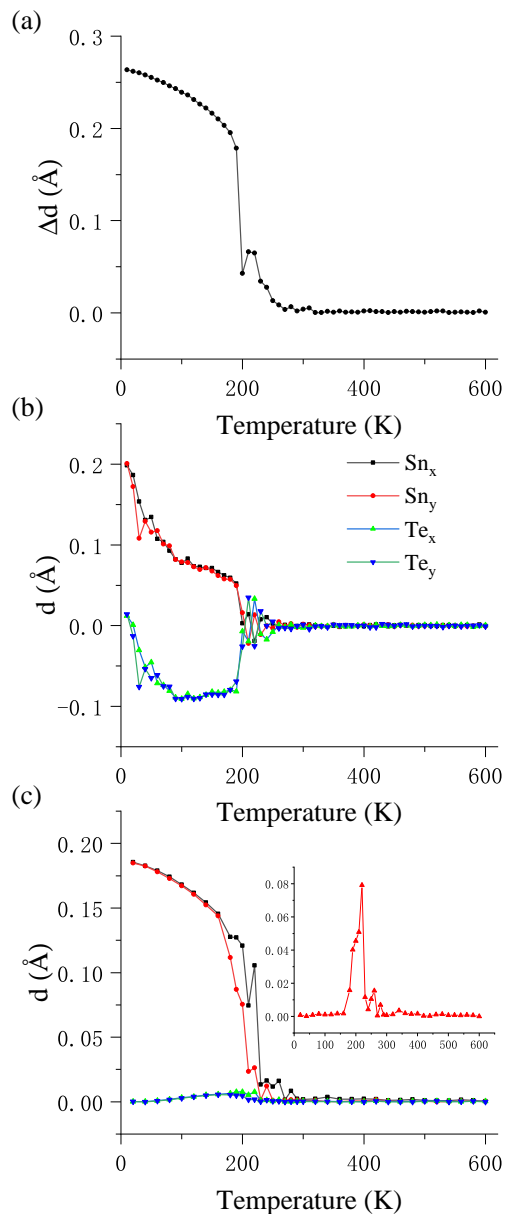


Figure 4. (a) Average relative displacement between Sn and Te atoms versus temperature (see Eq. (2)); (b) Average positions of Sn and Te atoms versus temperature; (c) Between 160K and 280K, the displacement of Sn atom is no longer exactly along the  $\langle 110 \rangle$  direction (see the text). The inset in (c) shows the displacement difference between the  $x$  and  $y$  directions.

Having constructed and trained the ANNs, we now employ them in MC simulations as energy calculators. The MC simulations use our home-brewed PyMC<sup>2</sup>, which is a modular Monte-Carlo simulation program specially designed for crystals<sup>33</sup>. In MC simulations, the ANNs are used to predict how much energy change arises when an atom is displaced. To find the phase transition temperature, we set up a 2D  $12 \times 12$  supercell (576 atoms), and gradually cool down the system from 600 K to 10 K with a step of 10 K. At each temperature, we sweep the systems 80,000 times, in each sweep all

atoms are displaced randomly and such moves are accepted or rejected depending on the incurred change of energy. Figure 4(a) shows the temperature evolution of the average relative displacement  $\Delta d$ , which is determined by the displacements of Sn and Te within the same unit cell, *i.e.*,

$$\Delta d = \frac{1}{N} \sum_{i=1}^N \langle |\mathbf{d}_{\text{Te}} - \mathbf{d}_{\text{Sn}}| \rangle, \quad (2)$$

where  $\langle \dots \rangle$  indicates the supercell average, and  $N$  is the number of MC sweeps used for the final average. As we can see from Fig. 4(a), a phase transition occurs at around 260 K, where the average displacement starts to increase with the decreasing temperature, gradually reaching a value around 0.26 Å. Figure 4(b) shows that the averaged displacement of Sn and Te separately, indicating that the relative displacements are along the  $\langle 110 \rangle$  direction. These results are consistent with the energy minimum at  $d = 0.26$  Å as shown in Fig. 3(c). They also indicate that the monolayer SnTe has a comparable phase transition temperature as the 1UC SnTe which are previously investigated both experimentally<sup>2</sup> and theoretically<sup>34</sup>.

Figures 4(a) and (b) also show that the Sn and Te atoms fluctuate violently around 200 K, which is likely due to the competition between the energy minimums (see Fig. 3). In order to understand the effects of the multiple energy minimums, we also simulated the system with slightly different setups. For Figs. 4(a) and (b), only the Te atom at the origin is fixed; for Fig. 4(c), we mimic the epitaxially strained SnTe structure by fixing the Te atoms at the corner of each unit cell (there are two Te atoms in each unit cell and one is fixed) so that the crystal lattice structure is fixed. As shown in Fig. 4(c), there is a narrow temperature range (between 160 and 280 K) where the displacement of Sn atom is no longer along the direction of  $\langle 110 \rangle$ , but more in the direction of  $\langle 100 \rangle$ . The snapshots of atom displacements indicate that, in this temperature range, there are Sn atoms shift along different  $\langle 110 \rangle$  directions, resulting in average displacement along the  $\langle 100 \rangle$  direction. Therefore, a second ferroelectric phase can be expected in the phase transition of monolayer SnTe, albeit it may only exist in a very narrow temperature range.

As mentioned before, the proposed approach can be transferred to a similar system, such as 2D monolayer GeTe. With the same procedure, we trained and tested ANNs for GeTe, which show excellent predictive abilities [see Figs. 5(a) and (b)]. With the ANNs, we again conducted MC simulations for monolayer GeTe, and found that GeTe, similar to SnTe, also have a structural phase transition with a phase transition temperature around 300 K as shown in Figs. 5(c) and (d). The phase transition temperature is higher than that of SnTe, consistent with the deeper potential well of GeTe.

In summary, we have adopted a ML approach to build and

train ANNs that are employed in MC simulations to investigate the structural phase transition of ferroelectric monolayer SnTe and GeTe. Unlike other approaches, no concrete model or formula, which often requires *a priori* knowledge or a good understanding of the given system, is necessary to approximate the PES, therefore also removing the difficulty in determining the coefficients, essentially resulting in a model-less

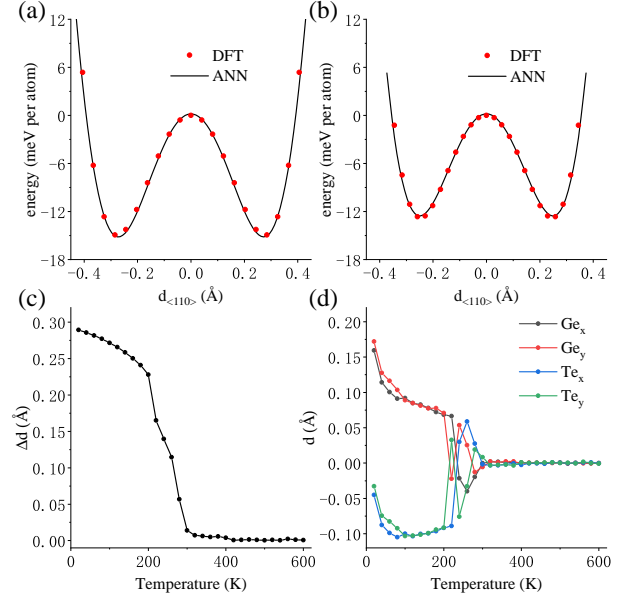


Figure 5. (a) and (b) shows the ANN's prediction results for GeTe; (c) Average relative displacement between Ge and Te atoms versus temperature; (d) Average position of Ge and Te atoms versus temperature.

approach while achieving accurate prediction of their phase transition temperature. It is demonstrated that the ANNs can work as a special universal mathematical structure that are capable for various systems as long as the training data from *ab initio* computation are available. Such virtues make the ML approach very general and flexible to investigate structural phase transitions of various systems.

## ACKNOWLEDGMENTS

This work is financially supported by the National Natural Science Foundation of China, Grant Nos. 11974268 and 12111530061. X.C. thanks the financial support from Academy of Finland Projects 308647. X.C. and D.W. thank the support from CSC (IT Center for Science, Finland), project 2001447, for providing computation resources. D.W. also thanks the support from the Chinese Scholarship Council (201706285020).

\* dawei.wang@xjtu.edu.cn

<sup>1</sup> J. F. Scott, *Applications of modern ferroelectrics*, Science **315**,

954–959 (2007).

<sup>2</sup> K. Chang, J. Liu, H. Lin, N. Wang, K. Zhao, A. Zhang, F. Jin, Y.

- Zhong, X. Hu, W. Duan, Q. Zhang, L. Fu, Q. Xue, X. Chen, S. Ji, *Discovery of robust in-plane ferroelectricity in atomic-thick SnTe*, Science **353**, 274 (2016).
- <sup>3</sup> L. W. Martin and A. M. Rappe, *Thin-film ferroelectric materials and their applications*, Nat. Rev. Mater. **2**, 16087 (2016).
  - <sup>4</sup> M. Dawber, K. M. Rabe, and J. F. Scott, *Physics of thin-film ferroelectric oxides*, Rev. Mod. Phys. **77**, 1083–1130 (2005).
  - <sup>5</sup> W. Kohn and L. J. Sham, *Self-Consistent Equations Including Exchange and Correlation Effects*, Phys. Rev. **140**, A1133 (1965).
  - <sup>6</sup> W. Zhong, D. Vanderbilt, and K. M. Rabe, *First-principles theory of ferroelectric phase transitions for perovskites: The case of BaTiO<sub>3</sub>*, Phys. Rev. B **52**, 6301 (1995).
  - <sup>7</sup> D. Wang, A. A. Bokov, Z.-G. Ye, J. Hlinka, and L. Bellaiche, *Sub-terahertz dielectric relaxation in lead-free Ba(Zr, Ti)O<sub>3</sub> relaxor ferroelectrics*, Nat. Commun. **7**, 11014 (2016).
  - <sup>8</sup> A. Al-Barakaty, S. Prosandeev, D. Wang, B. Dkhil, and L. Bellaiche, *Finite-temperature properties of the relaxor PbMg<sub>1/3</sub>Nb<sub>2/3</sub>O<sub>3</sub> from atomistic simulations*, Phys. Rev. B **91**, 214117 (2015).
  - <sup>9</sup> J. Zhang, Y. J. Wang, J. Liu, J. Xu, D. Wang, L. Wang, X. L. Ma, C. L. Jia, and L. Bellaiche, *Origin of sawtooth domain walls in ferroelectrics*, Phys. Rev. B **101**, 060103(R) (2020).
  - <sup>10</sup> J. Liu, L. Liu, J. Zhang, L. Jin, D. Wang, J. Wei, Z. G. Ye, and C. L. Jia, *Charge effects in donor doped perovskite ferroelectrics*, J. Am. Ceram. Soc. **103**, 5392 (2020).
  - <sup>11</sup> J. Behler, *Perspective: Machine learning potentials for atomistic simulations*, J. Chem. Phys. **145**, 170901 (2016).
  - <sup>12</sup> V. L. Deringer, M. Caro, and G. Csányi, *Machine learning interatomic potentials as emerging tools for materials science*, Adv. Mater. **31**, 1902765 (2019).
  - <sup>13</sup> Q. Tong, P. Gao, H. Liu, Y. Xie, J. Lv, Y. Wang, and J. Zhao, *Combining Machine Learning Potential and Structure Prediction for Accelerated Materials Design and Discovery*, J. Phys. Chem. Lett. **11**, 8710–8720 (2020).
  - <sup>14</sup> J. Behler, R. Martonak, D. Donadio, and M. Parrinello, *Metadynamics Simulations of the High-Pressure Phases of Silicon Employing a High-Dimensional Neural Network Potential*, Phys. Rev. Letter **100**, 185501 (2008).
  - <sup>15</sup> H. Eshet, R. Z. Khaliullin, T. D. Kuehne, J. Behler, and M. Parrinello, *Ab initio quality neural-network potential for sodium*, Phys. Rev. B **81**, 184107 (2010).
  - <sup>16</sup> J. Smith, O. Isayev, and A. E. Roitberg, *ANI-1: an extensible neural network potential with DFT accuracy at force field computational cost*, Chem. Sci. **8**, 3192–3203 (2017).
  - <sup>17</sup> F. Prudente, P. H. Acioli, and J. J. S. Neto, *The fitting of potential energy surfaces using neural networks: Application to the study of vibrational levels of H<sub>3</sub><sup>+</sup>*, J. Chem. Phys. **109**, 8801 (1998).
  - <sup>18</sup> D. F. R. Brown, M. N. Gibbs, and D. C. Clary, *Combining ab initio computations, neural networks, and diffusion Monte Carlo: An efficient method to treat weakly bound molecules*, J. Chem. Phys. **105**, 7597 (1996).
  - <sup>19</sup> A. P. Bartók, J. S. Kermode, N. Bernstein, and G. Csányi, *Machine Learning a General-Purpose Interatomic Potential for Silicon*, Phys. Rev. X **8**, 041048 (2018).
  - <sup>20</sup> G. Sosso, G. Miceli, S. Caravati, J. Behler, and Marco Bernasconi, *Neural network interatomic potential for the phase change material GeTe*, Phys. Rev. B **85**, 174103 (2012).
  - <sup>21</sup> J. Behler, *Representing potential energy surfaces by high-dimensional neural network potentials*, J. Phys.: Condens. Matter **26**, 183001 (2014).
  - <sup>22</sup> J. Behler and M. Parrinello, *Generalized Neural-Network Representation of High-Dimensional Potential-Energy Surfaces*, Phys. Rev. Lett. **98**, 146401 (2007).
  - <sup>23</sup> E. Prodan and W. Kohn, *Nearsightedness of electronic matter*, Proc. Natl. Acad. Sci. **102**, 11635–11638 (2005).
  - <sup>24</sup> S. Fiasa, F. Heidar-Zadeh, P. Geerlings, and P. W. Ayers, *Chemical transferability of functional groups follows from the nearsightedness of electronic matter*, Proc. Natl. Acad. Sci. U. S. A. **114**, 11633–11638 (2017).
  - <sup>25</sup> A. P. Bartók, R. Kondor, and G. Csányi, *On representing chemical environments*, Phys. Rev. B **87**, 184115 (2013).
  - <sup>26</sup> R. Hecht-Nielsen, *Theory of the backpropagation neural network*, IJCNN. (1989).
  - <sup>27</sup> W. Liu, Z. Wang, X. Liu, N. Zeng, Y. Liu, F. E. Alsaadi, *A survey of deep neural network architectures and their applications*, Neurocomputing **234**, 11–26 (2017).
  - <sup>28</sup> A. Paszke, et. al., *PyTorch: An Imperative Style, High-Performance Deep Learning Library*, NeurIPS (2019).
  - <sup>29</sup> J. Enkovaara et al., *Electronic structure calculations with GPAW: a real-space implementation of the projector augmented-wave method*, J. Phys.: Condens. Matter **22**, 253202 (2010).
  - <sup>30</sup> H. J. Monkhorst and J. D. Pack, *Special points for Brillouin-zone integrations*, Phys. Rev. B **13**, 5188 (1976).
  - <sup>31</sup> J. P. Perdew, K. Burke, and M. Ernzerhof, *Generalized Gradient Approximation Made Simple*, Phys. Rev. Lett. **77**, 3865 (1996).
  - <sup>32</sup> R. Cohen, *Origin of ferroelectricity in perovskite oxides*, Nature **358**, 136–138 (1992).
  - <sup>33</sup> The home-brewed Monte-Carlo program for crystals is hosted at <https://gitlab.com/dwang5/pymc2.git>
  - <sup>34</sup> Q. Ye, X. Zhang and X. Li, *The phonon-related effective Hamiltonian method for displacive ferroelectric materials*, Electron. Struct. **1**, 044006 (2019).